# Comparing Geometries for a PET System with 3-D Photon Positioning Capability

Garry Chinn, *Member, IEEE*, Angela M. K. Foudray, *Student Member, IEEE*, and Craig S. Levin, *Member, IEEE*

***Abstract*–We compared two PET system geometries, a box and a cylinder, for a novel PET 3-D detector design with axial, transaxial, and depth of interaction resolution of 1 mm, 1 mm, and 3 mm, respectively. Monte Carlo simulations have shown that arranging this detector into an 8x8x8 cm$^3$ FOV box has twice the sensitivity of a conventional cylinder of comparable dimensions (8 cm diameter, 8 cm axial length) due to a reduction in inter-module gaps. We compared image reconstruction performance for the box and the cylinder by computing the mean square error (MSE) for a weighted least squares estimator and contrast recovery coefficient (CRC) for rod phantoms with rods located at the radial center and radial offset of 2 cm. The contrast was comparable (near 100% CRC) for both box and cylinder. However, the cylinder showed slightly better contrast uniformity (CRC varied 2% for cylinder, 8% for box) as the radial position of the lesion was varied. The box had a MSE that was 7-14 times better than the cylinder system. We performed an ROC study by computing the detection SNR for computer observer models. A non-prewhitening and a prewhitening test statistic were computed to provide an upper and lower bound for the performance of human observers. The prewhitening filter detection SNR for the cylinder design was superior (by <15%) to the box at the center position. For all other source locations, the box showed an improvement (by >20%) in detection SNR. Finally, we reconstructed a resolution phantom with 3-D data for both systems and showed that both systems were qualitatively comparable.**

## I. Introduction

PET detectors are commonly deployed in a cylindrical geometry. For events in the direct planes, emissions from the center of the field of view are roughly perpendicular to the front face of each detector crystal. Emissions at a radial position away from the center can penetrate into adjacent crystals, creating depth of interaction positioning errors. The blurring caused by crystal penetration increases the further the radial position of the coincident detector pair is from the center. For conventional designs, the radius of the cylindrical system is generally chosen to be significantly larger than the field of view to improve resolution and depth blurring uniformity at the cost of reduced system sensitivity.

Manuscript received October 4, 2005. This work was supported in part by NIH grant R21 EB003283 from NIBIB.

G. Chinn is with the Department of Radiology, Stanford University, Stanford, CA. 94305-5344, USA (email: gchinn@stanford.edu).

A.M.K. Foudray is with the Department of Radiology, Stanford University and the Department of Physics, University of California, San Diego, La Jolla, CA, USA (email: afoudray@stanford.edu).

C.S. Levin is with the Department of Radiology, Stanford University, Stanford, CA. 94305-5344, USA (email: cslevin@stanford.edu).

We are currently developing a new detector technology with 3-D positioning capability [1]. This detector can be used to substantially reduce positioning errors caused by crystal penetration, allowing detectors to be positioned close to the imaging subject for increased sensitivity. Each detector module consists of 1 mm by 1 mm by 3 mm LSO crystals arranged in an 8 by 3 array side-coupled to position sensitive avalanche photodiodes (PSAPD). The PSAPD is arranged edge-on with respect to incoming photons. This arrangement provides 3 mm radial (depth of interaction) resolution and 1 mm transaxial and axial resolution.

PET systems are commonly constructed using rectangular detector modules arranged in a cylinder, leading to gaps between the detector blocks. We have shown that these gaps reduce sensitivity [2] by allowing photons to escape detection either by passing through the gaps without any interaction or by scattering from crystals into the gaps. Detectors arranged in a box have twice the center point sensitivity of a conventional cylindrical geometry system with a comparable diameter [2]. The increased sensitivity of the box geometry is attributable to the elimination of gaps between the detector blocks. However, a larger fraction of photons enter the detectors at oblique angles for the box geometry. For a cylindrical system, we can choose any $\xi$ and find a corresponding region of radius $r$ such that the blurring caused by crystal penetration of every line of response passing through this region is less than $\xi$. Such a "sweet spot" does not exist for the box geometry.

To evaluate and compare the designs, image reconstruction performance was assessed for different phantoms. In this study, we compared the box design against a cylinder using our novel detector modules. We compared the resolution and signal-to-noise ratio (SNR) of images reconstructed for various phantoms. We also performed a computer observer ROC study for lesion detection applications. Finally, a phantom was used to measure resolution performance.

## II. Method

We compared a box that was 8 cm in length on all sides and a cylinder with an 8 cm diameter and 8 cm axial length. The two systems are shown in Fig. 1. The 8 by 3 LSO-PSAPD arrays were stacked two-deep in the radial direction for a total crystal depth of 1.8 cm. The LSO crystals are coupled with a PSAPD array produced by RMD, Inc.

The PSAPD device is 11 mm by 11 mm with a sensitive area of 8 mm by 8 mm. The thickness of the device and flex cable package is < 0.3 mm. Depth of interaction resolution is provided by orienting the PSAPD arrays edge-on (radial

direction) with respect to incoming photons as shown in Fig. 2.

To compare the performance of the systems, the Monte Carlo simulation package GATE (GEANT4) [3] was used to simulate measurements of various phantoms. The noise properties of the two systems could have been studied by simulating multiple scans for each phantom. Reconstructed images for the different trials could then have been used to compute the mean square error and to perform ROC studies. However, such an approach would have required a prohibitive amount of computing resources since the GATE software is computationally intensive. Consequently, an alternative approach was pursued in this investigation.

The mean square error performance and the Fisher information matrix (FIM) can be computed directly from the system matrix. The FIM has previously been used for evaluating PET systems [4], [5] and can then be used to compute the ROC performance for computer observer models.

### A. System Model

PET imaging can be modeled by a system of linear equations. For our study, we used a simplified model taking into account only the geometric position and efficiency of the detectors in the form

$$\mathbf{y} = \mathbf{NPx} + \mathbf{n}$$

where $\mathbf{y}$ is the measurement (sinogram) vector, $\mathbf{x}$ is the activity distribution in the image volume, $\mathbf{n}$ is a random noise vector, $\mathbf{P}$ is the geometric projection matrix, and $\mathbf{N}$ is the normalization matrix. The geometric projection matrix was computed using Siddon's method [6].

We calculated the normalization matrix $\mathbf{N}$ by the direct method. A ring source was used for the cylindrical system and a box source for the box system. GATE was used to simulate normalization scans with an average of 44 counts per LOR.

### B. Signal-to-Noise Study

The SNR for penalized maximum likelihood (PML) reconstruction was estimated by a Gaussian approximation of the noise model with covariance $\mathbf{R} = \text{diag}(\mathbf{Px})$. In this case, the PML estimator becomes the weighted least squares solution

$$\hat{\mathbf{x}} = (\mathbf{P}^*\mathbf{R}^{-1}\mathbf{P})^{-1}\mathbf{P}^*\mathbf{R}^{-1}\mathbf{y}$$

with error covariance

$$\begin{aligned}\boldsymbol{\Sigma} &= \text{cov}(\hat{\mathbf{x}} - \mathbf{x}) \\ &= (\mathbf{P}^*\mathbf{R}^{-1}\mathbf{P})^{-1} \\ \text{mse} &= \text{trace}(\boldsymbol{\Sigma})\end{aligned}$$

Note that the Cramer-Rao bound is the inverse of the FIM and is simply

$$\mathbf{F}^{-1} = (\mathbf{P}^*\mathbf{R}^{-1}\mathbf{P})^{-1}.$$

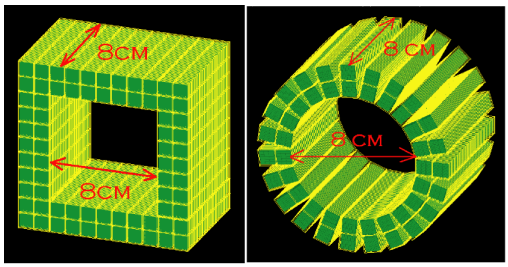


Fig. 1. These diagrams show the detector block arrangement for the box and cylindrical geometry under investigation. The LSO-PSAPD arrays are stacked two deep so that the effective crystal depth is 1.8 cm.

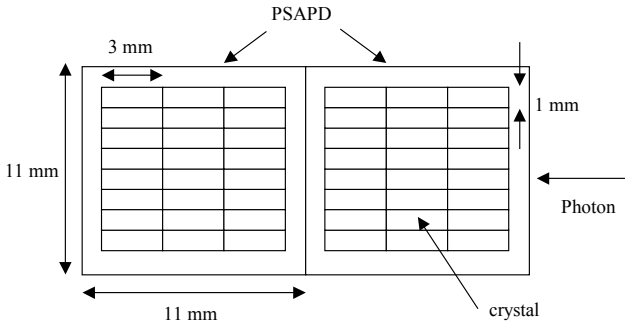


Fig. 2. This diagram shows the "edge on" layout of the crystals and PSAPD array in the proposed detector design. Two detector arrays are stacked in the radial direction to increase the intrinsic detection efficiency. The sensitive area of the PSAPD is 8 mm by 8 mm.

A fully three-dimensional PET system has a FIM that is too large for matrix inversion. Consequently, we restricted the FIM analysis to a two-dimensional box and cylindrical system.

### C. Lesion Detectability Study

Non-prewhitening (NPW) and prewhitening (PW) computer observers [4], [5] were used for a ROC study. A human observer is likely to perform within the range of these computer observers. If the reconstructed image is Gaussian distributed, the SNR of the test statistic is directly related to the area under the ROC curve (AUC) [4]. Hence, the SNR of the test statistic can be used as a proxy for AUC

$$\begin{aligned}SNR_{pw} &= (\mathbf{z}^*\boldsymbol{\Sigma}^{-1}\mathbf{z})^{1/2} \\ SNR_{npw} &= \mathbf{z}^*\mathbf{z}/(\mathbf{z}^*\boldsymbol{\Sigma}\mathbf{z})^{1/2} \\ \mathbf{z} &= h(f_l) - h(f_o)\end{aligned}$$

where $h(f_l)$ is the activity of the rod ROI and $h(f_o)$ is the activity of the background ROI.

### D. Phantom Study

To compare the signal-to-noise and lesion detection performance of the systems, a series of single lesion phantoms were simulated with GATE. A 2 mm diameter cylindrical rod was placed inside a 5 cm water cylinder with a 5:1 contrast ratio (lesion to background). The rod was placed at a radial position of 0 cm (center of cylinder) and 2 cm. Because of the asymmetries of the box, lesions were also placed along a

diagonal. For the cylindrical system, a lesion was simulated at just the center and offset at a radius of 2 cm.

### *E. Resolution Study*

We used a 3-D resolution phantom to measure the resolution capabilities of the two systems. This phantom consisted of 1.75, 1.5, 1.25, and 1 mm diameter sphere sources arranged in four different quadrants in the field of view. The spherical sources were separated by twice the diameter of the sources in each of the four quadrants. Images were reconstructed without normalization. The simulated scan time was 6 minutes with a total activity of 10 μCi in the phantom. The phantom consisted of spheres on three different planes located at z = 0 cm, z = 1.5 cm, and z = 3.0 cm. On each planes, spheres of 1.75 mm, 1.5 mm, 1.25 mm, and 1.0 mm were arranged in four quadrants.

## III. RESULTS

### *A. Reconstructed Images*

The ML-EM algorithm [7] was used to reconstruct images for all the 2-D phantom data. Fig. 3 shows the reconstructed images for the various point source lesions.

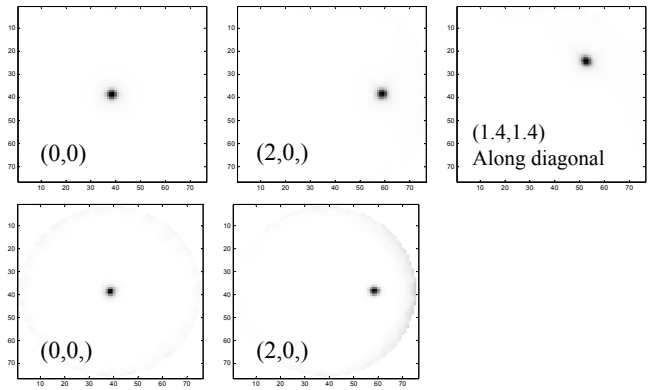


Fig. 3. Shown are the images reconstructed by ML-EM (maximum likelihood expectation maximization) for the (top row) box geometry with a lesion at (0,0), (2.0,), (1.4,1.4) cm and for the (bottom row) ring geometry (1st two locations only).

Fig. 4 shows the reconstructed images for the high-resolution 3-D phantom. The high-resolution phantom was reconstructed using the ordered subset list-mode EM algorithm [8] for a fully 3-D data set with 0.5 mm voxels. Both systems were capable of resolving the 1 mm spheres.

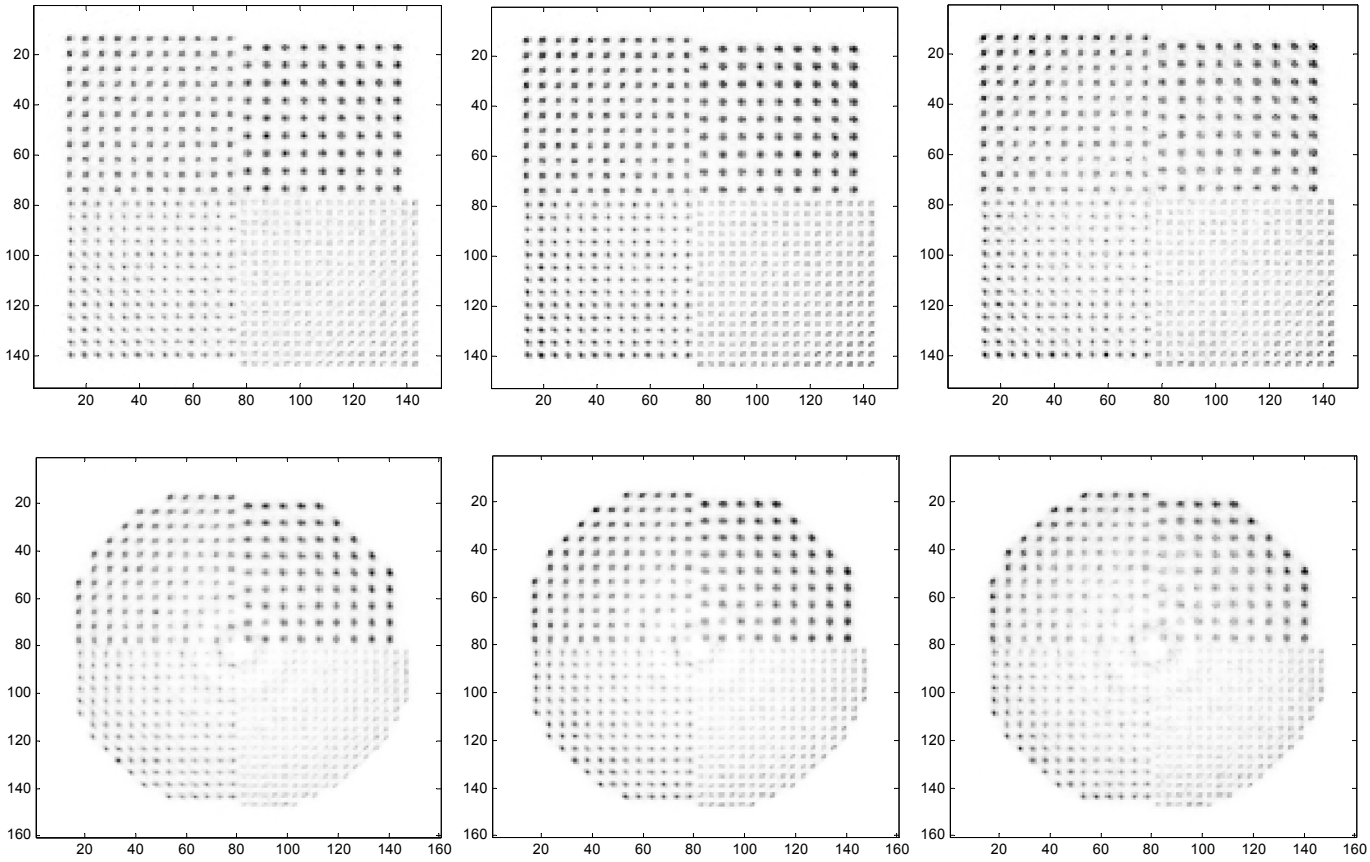

Fig. 4. A resolution phantom was reconstructed using the list-mode OS-EM algorithm with 0.5 mm voxels for the box (left column) and cylinder (right column) using one iterations and 8 subsets without attenuation correction or normalization. Data was simulated with GATE for a fully 3-D data acquisition system. A total scan time of 4 minutes was simulated. The total activity in the phantom was 10 μCi. Three planes of spheres were located at (top row) z = 0 (center axial plane), (middle) z = 1.5 cm, and (bottom) z = 3.0 cm. The spheres in the four quadrants (1 to 4) were 1.75, 1.5, 1.25, and 1.0 mm in diameter and spaced center-to-center at twice the diameter of the spheres.

### A. Mean Square Error and Contrast Recovery

The mean square error was computed for the single lesion phantoms along with the contrast recovery coefficient. The results are shown in Table I. Since the cylinder is circularly symmetric, the lesion at (1.4,1.4) cm provides redundant information and was not necessary for this evaluation. The MSE was normalized to the (0,0) lesion for the cylinder geometry and is presented in arbitrary units. The box geometry showed a 7-14 times improvement in mean square error performance compared to the cylinder geometry. The contrast recovery for the box system was fairly uniform. However, the contrast recovery was 9% more uniform for the cylinder geometry with the box geometry showing the poorest contrast recovery when the single rod was located at the center of the field of view.

### B. Computer Observer ROC Study

The SNR for the PW filter and NPW filter test statistics were computed for the various single lesion phantoms. The results of this study are tabulated in Table II. All results are normalized to the PW filter for the center lesion in the cylinder geometry.

The PW and NPW test statistic provide an estimate of the lower and uppers bounds of human observers. The cylinder geometry had a better detection PW SNR for the phantom with activity at the center of the field of view while the box geometry had a better PW SNR for phantoms with activity distributed closer to the detectors. The box geometry had a better NPW SNR for all rod locations.

## IV. Discussion and Conclusions

We used analytic approaches to compare the performance of the box and cylinder using analysis of the 2-D FIM. The cylinder geometry slightly outperformed the box geometry for single rod phantoms with activity at the center of the field of view. However, for simple phantoms with activity distributed away from the center of the field of view, the box geometry was superior in terms of MSE, CRC, and lesion detection applications.

We also reconstructed a more complex resolution phantom using fully 3-D data to demonstrate that both systems can reconstruct artifact-free images. Due to 3-D positioning capabilities of the proposed detectors, both designs were capable of resolving the 1 mm spheres even when positioned very near to a detector.

TABLE I
THE MEAN SQUARE ERROR (MSE) AND CONTRAST RECOVERY COEFFICIENT (CRC) WERE CALCULATED FOR SINGLE LESION PHANTOM WITH LESION LOCATED AT DIFFERENT (X,Y) POSITIONS IN CM FOR THE CYLINDER AND THE BOX

| | Cylinder geometry | | Box geometry | | |
|---|---|---|---|---|---|
| | (0,0) | (2,0) | (0,0) | (1.4,1.4) | (2,0) |
| MSE | 1.0 | 1.39 | 0.14 | 0.11 | 0.10 |
| CRC | 1.0 | 0.98 | 0.92 | 1.0 | 0.99 |

TABLE II
THE COMPUTER OBSERVER SIGNAL-TO-NOISE RATIO FOR THE PREWHITENING FILTER TEST STATISTIC (SNR PW) AND THE NON-PREWHITENING FILTER TEST STATISTIC (SNR NPW) FOR THE SINGLE LESION PHANTOMS WERE COMPUTED FOR LESION DETECTION AT DIFFERENT RADIAL POSITIONS.

| | Cylinder geometry | | Box geometry | | |
|---|---|---|---|---|---|
| | (0,0) | (2,0) | (0,0) | (1.4,1.4) | (2,0) |
| SNR PW | 1.0 | 0.57 | 0.84 | 0.75 | 0.77 |
| SNR NPW | 0.02 | 0.01 | 0.13 | 0.11 | 0.10 |

Unlike the single lesion phantoms, the two systems for the complex resolution phantom were qualitatively comparable even though the cylinder system had fewer than ½ the counts of the box system. There was a bull's eye artifact in the cylinder system. It is unclear whether this is an artifact of the circular phantom or of the system. We believe that normalization will correct this artifact.

It is clear that performance is highly phantom dependent and therefore, it will be necessary to characterize the system performance for specific applications by choosing appropriate phantoms. The single lesion phantoms used in this study are too simplistic and do not accurately reflect real world applications. It is unclear whether the box geometry will improve image quality for realistic phantoms. However, the box design does appear to be at least comparable to the cylindrical design with twice the sensitivity for a center point source and is easier to build and calibrate.

## References


[1] C.S. Levin, A.M.K. Foudray, P.D. Olcott, and F. Habte, "Investigation of position sensitive avalanche photodiodes for a new high-resolution PET detector design" *IEEE Transactions on Nuclear Science*, 51 (3): 805-810, 2004.

[2] A. M. K. Foudray, F. Habte, G. Chinn , J. Zhang, C. S. Levin, and P. D. Olcott, "Optimization of a Cylindrical PET Breast Imaging System Comprised of Position Sensitive Avalanche Photodiodes Utilizing Monte Carlo Simulation, " Presented at the 2004 IEEE Breast Imaging Workshop, Oct 22-24, 2004, Roma, Italy.

[3] D. Strul, G. Santin, D. Lazaro, V. Breton and C. Morel, "GATE (Geant4 Application for Tomographic Emission): a PET/SPECT general-purpose simulation platform," *Nucl. Phys. B (Proc. Suppl.)* vol. 125 (2003) 75-79

[4] H.H. Barrett, "Objective assessment of image quality: effects of quantum noise and object variability*," JOSA A*, vol. 7, pp. 1266-1278, July 1990.

[5] J. Qi and R.H. Huesman, "Theoretical study of lesion detectability of MAP reconstruction using computer observers," *IEEE Trans. Med Imaging*, vol. 20, pp. 815-822, 2001.

[6] R.L. Siddon, "Fast calculation of the exact radiological path for a three-dimensional CT array," *Med. Phys*., vol. 12, pp. 252-255, 1985.

[7] L.A. Shepp and Y. Vardi, "Maximum likelihood reconstruction for emission tomography," *IEEE Trans. Med. Imaging*, vol. 1, pp. 113-122, 1982.

[8] L. Parra and H.H. Barrett, "List-mode likelihood: EM algorithm and image quality estimation demonstrated on 2-D PET," *IEEE Trans. Med. Imaging*, vol.17, pp. 228-235, 1998.